A fast fault diagnosis method of the PEMFC system based on extreme learning machine and Dempster-Shafer evidence theory

Jiawei Liu, Qi Li, *Senior Member, IEEE,* Weirong Chen, *Senior Member, IEEE,* Yu Yan, Xiaotong Wang

***Abstract*—For purpose of solving the data-driven failure diagnosis problems of the proton exchange membrane fuel cell (PEMFC) system, improve the test accuracy and shorten the training time, a novel failure diagnosis method of the PEMFC systems based on data fusion is proposed, which combines extreme learning machine (ELM) and Dempster-Shafer evidence theory. The characteristic vector extraction is carried out on the electrical quantities and the non-electrical quantities of the PEMFC system under four different faults. The kernel extreme learning machine (K-ELM) algorithm and online sequential extreme learning machine (OS-ELM) algorithm are respectively used to establish the failure diagnosis model of PEMFC system based on electrical quantities and non-electrical quantities. It is used for preliminary failure diagnosis of a PEMFC system. The diagnosis results of the above two strategies are converted into the function values of the basic probability assignment (BPA) by the squeeze function. The Dempster-Shafer evidence theory algorithm is used to fuse the diagnostic output at the decision level. The classification results of 154 samples of PEMFC system show that the novel model can diagnose four different degrees of high air stoichiometry failures. The average recognition rate is 98.70% and the operation time is only 0.2011 s. At the same time, the comparisons with the back-propagation neural network (BPNN) and one-against-one support vector machine (SVM) show that the data fusion algorithm can significantly improve the running speed while ensuring the correct recognition rate. It can be used for online failure diagnosis of the PEMFC systems.**

***Index Terms*—PEMFC, data fusion, Dempster-Shafer evidence theory, fault diagnosis, online sequential extreme learning machine, kernel extreme learning machine.**

I. Introduction

PEMFC has the advantages of zero-emission, low vibration, low operating temperature, low noise, and high efficiency [1-3]. PEMFC system has excellent potential for application in various fields, including transportation, distributed generation, backup power, and power supply for portable devices [4-6]. In particular, PEMFCs are increasingly considered as an alternative to the internal combustion engine as the primary energy conversion device when the global energy environment is becoming more and more severe [7-9].

Manuscript received August 16, 2018; revised November 3, 2018; accepted December 3, 2018. This work was supported by National Natural Science Foundation of China (61473238), National Key Research and Development Program of China (2017YFB1201003-019), NEEC Open-end Fund of China (NEEC-2017-B01). (Corresponding author: Qi Li.)

The authors are with the School of Electrical Engineering, Southwest Jiaotong University, Chengdu 611756, China (e-mail: daben@my.swjtu.edu.cn; liqi0800@163.com;wrchen@swjtu.edu.cn;651467057@qq.com;624656069@qq.com).

Although much work has been done in promoting PEMFC technology and significant progress has been made in the past decades, there are still some dares that need to be got over [10]. For the PEMFC system itself, durability and cost are two key hurdles [11-13].

Fault diagnosis is an essential part of the operation and management of the PEMFC system [14]. Fault diagnosis and isolate (FDI) has received more and more attention at present. Through fault detection and early warning, more serious failures can be prevented. According to the diagnosis result, the operating conditions are oriented to make the PEMFC operate safely and efficiently. Accurate diagnostic information can facilitate the development of updated technologies and shorten downtime (maintenance time). The failure diagnosis is playing a more and more critical role in the modern industrial system. Many experts and scholars have conducted much research on failure diagnosis strategies for PEMFC system. These works can be divided into two classifications:

1) The model-based failure diagnosis method [15]

First, a PEMFC model is established, which involves an analytic model or a black box model. Then the real-time deviation between the actual PEMFC system and the expected health behavior is calculated. Finally, faults can be detected in real time through residual analysis. However, it is complicated to establish an accurate fault diagnosis model because the internal parameters, structure, and materials of PEMFC are challenging to obtain.

In addition to model-based fault diagnosis methods, data-driven diagnostic methods have also attracted the attention of researchers.

2) The data-driven failure diagnosis method

Data-driven diagnosis method uses historical data of monitoring to detect and identify faults. It does not need a PEMFC model and system expertise. The underlying algorithm is fast and computationally efficient. D. Ritzberger et al. [16] have presented a data-driven identification approach based-on Volterra series and nonlinear autoregressive models (NARX) with external inputs. This method can figure the dynamic behavior, current characteristics and nonlinear voltage of the PEMFC. The time-domain NARX matrix is transformed into a Volterra series presentation by harmonic detection arithmetic. The linear and non-linear dynamic frequency domain descriptions are obtained. By assessing the difference between the analog output value and the measured value, the time-domain NARX matrix can be used for failure detection. Zhongliang Li et al. [17] have proposed an SVM based fault

diagnosis strategy for PEMFC system. In this strategy, fourteen single cell voltages are used as diagnostic variables. The embedded system is used to monitor each cell voltage and perform the diagnostic algorithm. It can detect and isolate four kinds of faults online in real time. Xingwang Zhao et al. [18] have presented a fault detection approach based on the principal component analysis (PCA) and multi-sensor signals. This method analyses the correlation between different sensor symbols and deduces a simplified fault diagnosis statistic indicatrix, which can diagnose serious system-level failure and single sensor failure. Zhixue Zheng et al. [19] have put forward a method for PEMFC failure diagnosis based-on reservoir computing (RC). The experimental consequences prove that the RC medium can differentiate four kinds of health states, such as natural degeneration, poor cooling, low air flow rate, and carbon monoxide poisoning. Meng Shao et al. [20] have presented the failure diagnosis approach of the PEMFC backup power supply based on an artificial neural network (ANN) ensemble. For faults in air-cooled fuel cells, the faults are divided into four types: fuel cell anode flooding faults, hydrogen gas permeability improvement faults, coolant subsystem faults, and hydrogen supply subsystem faults. The parameters of the total voltage of the PEMFC stack, monomer cell voltage, fuel cell output current, anode gas inlet pressure, and hydrogen flow rate are used as inputs of the ANN ensemble method. The Bagging algorithm is used to generate the different neural network from the data sample. The training samples of various faults learn the individual neural network. The trained four individual neural networks are merged through the decision network. Compared with the fault diagnosis strategy of BPNN, the ANN ensemble fault diagnosis method can greatly improve the fault diagnosis rate. The diagnostic accuracy is increased from 84.34% to 93.21%. Jiawei Liu et al. [21] have proposed a discrete hidden Markov model (DHMM) failure diagnosis strategy based on K-means clustering of PEMFC systems of tramways. The considered fault categories involve deionized humidification pump low pressure, deionized glycol high inlet temperature, low air pressure, normal state, deionized glycol outlet temperature signal voltage over the range, and hydrogen leakage. The diagnostic results indicate that the six considered faults can be diagnosed and the fault recognition correct rates with the novel scheme are at most 94.17%. Literature [22, 23] has presented a failure diagnosis approach of PEMFC systems which considers the system dynamics and the spatial inhomogeneity. The voltages of the fourteen-monocell are chosen as the diagnostic variables during the sliding window. The shapelet transform accomplishes the feature extraction process. The procedure of fault diagnosis and isolation is carried out by the sphere shaped multi-class support vector machine (SSM-SVM). The effectiveness and robustness of the novel strategy are verified by the 4 kW PEMFC experiment test with the classification accuracy of 96.13% for five health states. Lei Mao et al. [24-27] have developed a choice algorithm of the sensor and inquired into its application on the online diagnosis of PEMFC. The proposed method considers the aging rate and sensor errors. The comparison with the noise-resistance based approach and the exhaustive searching method shows that the results of the novel strategy are the most efficient selection method of sensors with less computational complexity. H. Detti et al. [28] have presented a failure diagnosis approach of PEMFC based on the fast Fourier transform (FFT) and total Harmonic distortion (THD), in which two types of failures (membrane drying and flooding) can be judged of. R. Petrone et al. [29] have investigated the change process of the stack voltage under the operations of poor water management and lack of reactant. A multi-fault diagnosis method of double-fuzzy clustering is presented with the measurements of electrochemical impedance spectroscopy (EIS). Gianluigi Buonocunto et al. [30] have successfully detected the water flooding and membrane drying based on the Kalman filter (KF) method. The novel approach adopts the waveforms of time-domain to recognize three coefficients (1 capacitance and 2 resistances) from the simplified equivalent circuit model (ECM) of the PEMFC. The KF strategy has the advantages of the low calculated amount and easy to implement. E. Pahon et al. [31, 32] have presented a wavelet transform (WT)-based failure diagnosis method. The proposed approach can detect and identify the high air stoichiometry (HAS) failure of PEMFC.

However, the traditional PEMFC fault diagnosis method is mainly used to diagnose single-cell, small and medium-power PEMFC stacks. The research on failure diagnosis of a PEMFC system for high-power transit buses and light rail vehicles is almost blank [33]. Traditional methods of fuel cell fault diagnosis have the disadvantages of high computational complexity, long training time and complex parameter adjustment process. Achieving real-time synchronization of multi-channel data and decision-making system is confusing. In practice, the failure diagnosis of the PEMFC system by the traditional method may expend much computation time and increase the computation complexity. Therefore, it is necessary to integrate the results of other fault diagnosis methods to reduce computation time and improve the diagnostic accuracy.

SVM has the deficiencies of the limited kernel function, large sample demand and the low algorithm convergence. BPNN mostly adopts the gradient descent method. BPNN mainly has the disadvantages of easy to fall into a local minimum, moderative training speed, unable to achieve global minimum and sensitive selection of learning rate. ELM randomly creates the connection weights between the hidden layer and the input layer, and the thresholds at the hidden layer neurons. At the training process, the unique optimal solution can be obtained by setting the number of hidden layer neurons. Compared with the present training methods, ELM has the benefits of fast-learning speed and good universalization performance. ELM is fast training arithmetic for a single hidden layer neural network. ELM casually selects the weights and offsets of the hidden-layer nodes. It can determine the network parameters without any iterative steps, which can significantly reduce the settling time of the network parameters. ELM is widely used in wind power generation, electricity price forecast, traffic street sign identification and handwriting recognition [34]. At present, there is no literature to apply ELM to the field of PEMFC fault diagnosis.

In this paper, a fast failure diagnosis approach based on ELM algorithm and D-S evidence theory dedicated to the PEMFC system is proposed for the first time. The characteristic vector extraction is carried out on the electrical quantities and the non-electrical quantities of the PEMFC system under four different faults. The K-ELM algorithm and OS-ELM algorithm are respectively used to establish the fault diagnosis model of the PEMFC system based on electrical quantities and non-electrical quantities. It is used for preliminary failure diagnosis of the PEMFC system. The diagnosis results of the above two strategies are converted into the function values of the BPA by the squeeze function. The D-S evidence theory algorithm is used to fuse the diagnostic output at the decision level. The feasibility of the novel method is validated by 154 samples of four different degrees of high air stoichiometry faults. The results are compared with the traditional one-against-one SVM algorithm and BPNN algorithm to verify the effectiveness of the novel algorithm.

II. Description of the PEMFC System

A. Description of the 14.4 kW Liquid-cooled PEMFC Test Bench

The 14.4 kW liquid-cooled PEMFC test platform is shown in Fig. 1.

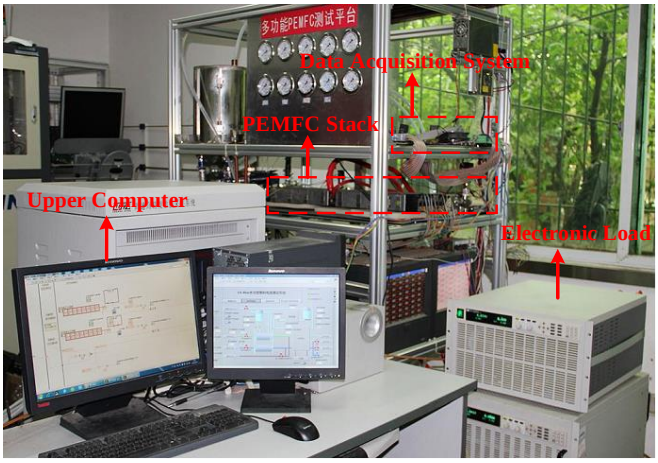

Fig. 1 Photo of the 14.4 kW liquid-cooled PEMFC test platform [35]

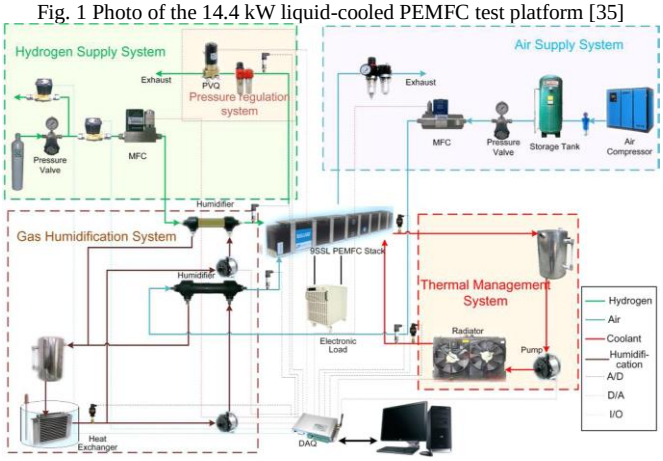

Fig. 2 Schematic diagram of the PEMFC test platform [35]

The principle is shown in Fig. 2. The entire PEMFC system includes a PEMFC stack and the following subsystem: hydrogen supply subsystem, air-supply subsystem, regulation subsystem of anode back pressure, humidification heating subsystem, thermal management subsystem, single cell voltage acquisition subsystem and test platform control subsystem. The parameters can be monitored summed in Table 1.

Table 1 Measured parameters

Parameter	Symbol
The flow rate of the H_2 inlet	F_{in,H_2}
The pressure at the H_2 inlet	P_{in,H_2}
The temperature at the H_2 inlet	$T_{in.H_2}$
The flow rate of the air inlet	$F_{in,air}$
The pressure of the air inlet	$P_{in,air}$
The temperature of the air inlet	$T_{in,air}$
The flow rate of the coolant inlet	$F_{in,water}$
The pressure at the coolant inlet	$P_{in,water}$
The temperature at the coolant inlet	$T_{in,water}$
The temperature at the coolant outlet	$T_{out,water}$
The current	I
The stack voltage	V_s
The N *th* cell voltage (N =1, 2,…, 75)	V_N
Fan control voltage	V_{fan}
Pump control Voltage	V_{pump}
Ambient temperature	$T_{ambient}$
The temperature at the radiator inlet	$T_{in,radiator}$

The air and hydrogen flow rates are regulated by changing the valve opening of the air MFC and hydrogen MFC. The flow rate of the coolant and the differential temperature between the outlet and the inlet of the coolant can be adjusted by changing the speed of the coolant pump. The inlet temperature of the coolant can be adjusted by changing the speed of the radiator fan. The humidifies of inlet air and hydrogen can be adjusted by changing the speed of the humidification pump. The pressure at the hydrogen inlet can be adjusted by changing the opening of the anode outlet proportional solenoid valve. The acquisition and control of related physical quantities are accomplished through the analog input and output channel of the acquisition card. The digital input and output function of the acquisition card is used to monitor and control the corresponding switch devices and alarm devices.

B. Experimental Protocols

The high purity hydrogen (> 99.999%) of the high-pressure gas tank enters into the PEMFC anode after decompression. The pressurized air in the air compressor enters the PEMFC cathode through the gas buffer tank. The MFCs precisely regulate the flow rates of air and hydrogen. The coolant pump transfers coolant to the radiator from the outlet of the stack. The coolant temperature is precisely adjusted by varying the fan speed. During the period of running, a multi-channel data gathering system can monitor the voltage information of seventy-five single cells at all hours. Ballard Power Systems Inc. supplies the protocols to start, stop and operate the FCvelocity®-9SSL V4 PEMFC stack. Some crucial steps must be followed up to avert damages on the PEMFC stack (such as H_2/O_2 reactions on the anode, fuel starvation, extreme temperatures, and other unstable events). Fuel cell failure will

weaken the service life of the fuel cell system. When the given air dew point temperature is accomplished, the PEMFC can operate in the nominal running conditions, as shown in Table 2. From that moment on, all variables are recorded in the nominal running conditions. This operating condition is considered a healthy operating mode. Therefore, when the operating conditions are changed, the fuel cell stack may run in failure mode. The more deviation is between the actual operating conditions and the nominal operating conditions, the more serious the failure of the PEMFC system is. The failure considered in this paper is the variation of the air excess coefficient. This failure may be related to the misfunctioning of the air compressor. The receivable ranges for the various running parameters of the PEMFC are shown in Table 3.

Table 2 Nominal operating conditions

I/A	$\lambda_{\min,H_2}$	P_{in,H_2} /kPa	$\lambda_{\min,air}$	$P_{in,air}$ /kPa	$T_{in,water}$ /°C	$T_{out,water}$ /°C
15	6.3	115	5.1	108	60	61
30	3.4	116	2.4	110	60	63
60	2.2	131	1.8	117	60	66
120	1.9	155	1.8	138	60	67
180	1.6	179	1.8	158	60	68
240	1.6	200	1.8	180	60	68
300	1.6	220	1.8	200	60	70

Footnotes: I is stack current; $\lambda_{\min,H_2}$ is minimum inlet hydrogen stoichiometry; P_{in,H_2} is rated pressure at the hydrogen inlet; $\lambda_{\min,air}$ is minimum inlet air stoichiometry; $P_{in,air}$ is rated pressure at the air inlet; $T_{out,water}$ is maximum coolant outlet temperature; $T_{in,water}$ is maximum coolant inlet temperature; $P_{in,water} \le P_{in,air}$, where $P_{in,water}$ is rated pressure at the coolant inlet; $D_{\min,water}$ =0.05 L/min/cell, where $D_{\min,water}$ is minimum coolant flow rate.

Table 3 Stack operating limits [36]

Condition	Limit	Reason
Maximum allowable working pressure	350 kPa (abs)	Stack integrity
Minimum allowable reactant cross pressure (steady state)	7 kPa to 20 kPa	Cell stability, safety
Maximum allowable reactant cross pressure (steady state)	50 kPa	Stack damage
Maximum allowable cross pressure–anode to the coolant (steady state)	100 kPa	Stack damage
Maximum allowable coolant outlet temperature	70 °C	Stack integrity
Maximum allowable coolant temperature differential (steady state)	10 °C	Stack integrity
Maximum allowable reactant inlet temperature (steady state)	68 °C	Stack damage
Maximum allowable coolant outlet temperature	70 °C	Stack integrity
Minimum recommended operating cell voltage (steady state)	0.2 V	Stack lifetime
Maximum recommended cell voltage	0.85 V	Stack lifetime
Individual cell variability from the average cell voltage	80 mV	Stack lifetime
Maximum sustained stack current	300 A	Stack specification

During the operation of the PEMFC stack, the hydrogen stoichiometry has little effect on the performance of the stack. However, the variation of air stoichiometry has a significant effect on the output performance of PEMFC. The steady-state output performance of PEMFC stack is experimentally tested under different air stoichiometries. The output current of the stack is kept constant at 50 A during the experiment. The experimental parameters are shown in Table 4.

Table 4 Experimental parameters

Parameter	Value
Coolant temperature differential	5 ℃
Coolant inlet temperature	60 ℃
The temperature at the air inlet	60 ℃
The temperature at the H_2 inlet	60 ℃
Stack current	50 A
Hydrogen stoichiometry	2.6
Gas relative humidity	≥ 95%
The pressure difference between anode and cathode	10 kPa

When the air stoichiometries are 5.1, 4.6, 4.2 and 2.1 respectively, the average voltage distributions of the single cell voltage of the PEMFC stack in the four cases are presented in Fig. 3. The horizontal axis expresses the 75-single cell, and the vertical axis expresses the voltage distributions during four different air stoichiometries. As can be seen from Fig. 3, the setting of the air stoichiometry is closely related to the stack output performance.

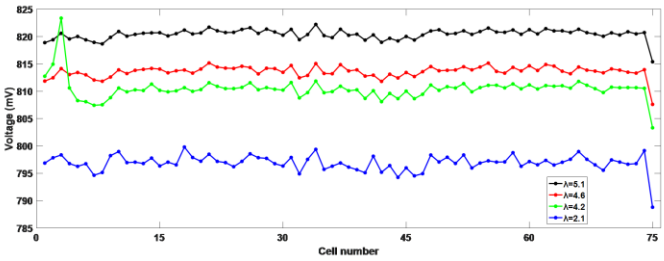

Fig. 3 Voltage distribution of single cell under different air stoichiometries

In the output state of 50 A (the optimal air stoichiometry is 2.1), the single cell voltage increases slightly with the increase of air stoichiometry. The increase of air stoichiometry is beneficial to improve the voltage output performance of a single cell in the PEMFC stack. Under the conditions of different air stoichiometries, the voltage value of the 75*th* single cell is the lowest. The FCvelocity®-9SSL V4 stack is a PEMFC stack of the co-flow structure. A co-flow fuel cell stack is one in which both reactant streams and the coolant streamflow in the same direction across the cell. The 75*th* single cell is located on the edge of the stack and near the inlet and outlet side of the fluid. The temperature and flow rate of the 75*th* single cell is the lowest, so the 75*th* single cell has a lower output voltage relative to other positions.

The effectiveness and generalization of the experiments are needed to be verified carefully. References [27, 28] have paid high attention to a little-noticed failure: high air stochiometry failures. A 40-cell PEMFC system accomplishes the experiment. The air excess coefficients are set 2, 4 and 5 respectively under steady-state operating conditions. The generalization ability and the robustness of the experiments have been testified.

C. Impact of the High Air Excess Coefficient Failure on the Performance of the PEMFC System

1) Rupture of the PEM

When the air stoichiometry improves, the pressure at the air inlet also increases. Ballard recommends operating the stack with the anode pressure higher than the cathode to avoid possible fuel starvation. Nitrogen cross-over grades from the cathode to the anode improve as cathode pressure improves

relative to the anode pressure. Engaging the pressure of cathode is lower than the pressure of anode will improve cell stability and minimize nitrogen cross-over.

Furthermore, from a safety perspective, it is preferred to run the anode at the higher pressure than the cathode. In the event of an internal leak, hydrogen would preferentially leak to the cathode and be diluted by the air, or combine with oxygen to produce water. When the pressure at the air inlet is too high, the gas pressure difference between the anode and the cathode of the PEM also gradually increases. When the gas pressure difference between the cathode and the anode exceeds the allowable working range of the PEM, it may damage the PEM and even lead to the rupture of the PEM.

2) Drop in the Output Voltage of the PEMFC

In the fuel cell system, although the gas-liquid humidification process has humidified the gas inside the fuel cell, the water on the PEM may be taken out of the cell by excessive flow rate at the air inlet. As a result, the water content in the PEM decreases, and the membrane drying failure occurs. The low water content will seriously affect the proton conductivity. It may lead to the increase of ohmic potential and the decrease of the stack output voltage.

3) Efficiency Reduction of Power Generation System

From the perspective of the actual fuel cell system, air is mainly provided by the air compressor. When the oxygen flow rate is much higher than the demand, the excessive air stoichiometry will increase the burden of the air compressor and consume more energy. The power consumption of the air compressor is too large, and the output power of the stack is not improved obviously, which will significantly reduce the efficiency of the whole power generation system. The too much parasitic loss is a severe problem for the fuel cell system with limited power.

III. Fault Diagnosis Model of PEMFC System Based on K-ELM and OS-ELM

When the fuel cell system fails, its electrical quantity parameters and non-electrical quantity parameters all have different degrees of change. Each parameter is used as the characteristic information. The problem of fault diagnosis can be considered as the complex nonlinear pattern recognition problem. The K-ELM algorithm and the OS-ELM algorithm are applied to the failure diagnosis of the PEMFC system.

A. Kernel Extreme Learning Machine

For multi-output ELM based-on constrained optimization, the multi-classification problem can be expressed as:

Minimize:

$$L_{P_{ELM}} = \frac{1}{2}\|\boldsymbol{\beta}\|^2 + \frac{C}{2}\sum_{i=1}^{N}\|\boldsymbol{\xi}_i\|^2 \tag{1}$$

Constraint condition:

$$\mathbf{h}(\mathbf{x}_i)\boldsymbol{\beta} = \mathbf{t}_i^T - \boldsymbol{\xi}_i^T,\ i = 1,2,\mathbf{L}\ ,N \tag{2}$$

Where $\boldsymbol{\xi}_i = [\xi_{i1}, \xi_{i2}, \mathbf{L}\ , \xi_{im}]^T$ are the training error vector corresponding to the input data $\mathbf{x}_i$; C is the compromise parameter. According to the Karush-Kuhn-Tucker (KKT) mechanism, the training of ELM is equal to solving the following double optimization problem:

$$L_{D_{ELM}} = \frac{1}{2}\|\boldsymbol{\beta}\|^2 + \frac{C}{2}\sum_{i=1}^{N}\|\boldsymbol{\xi}_i\|^2 - \sum_{i=1}^{N}\sum_{j=1}^{m}\alpha_{ij}(\mathbf{h}(\mathbf{x}_i)\boldsymbol{\beta}_j - t_{ij} + \xi_{ij}) \tag{3}$$

The identical optimization conditions of KKT are as follows:

$$\frac{\partial L_{D_{ELM}}}{\partial \boldsymbol{\beta}_j} = 0 \rightarrow \boldsymbol{\beta}_j = \sum_{i=1}^{N}\alpha_{ij}\mathbf{h}(\mathbf{x}_i)^T \rightarrow \boldsymbol{\beta} = \mathbf{H}^T\boldsymbol{\alpha} \tag{4}$$

$$\frac{\partial L_{D_{ELM}}}{\partial \boldsymbol{\xi}_i} = 0 \rightarrow \boldsymbol{\alpha}_i = C\boldsymbol{\xi}_i,\ i = 1,2,\mathbf{L}\ ,N \tag{5}$$

$$\frac{\partial L_{D_{ELM}}}{\partial \boldsymbol{\alpha}_i} = 0 \rightarrow \mathbf{h}(\mathbf{x}_i)\boldsymbol{\beta} - \mathbf{t}_i^T + \boldsymbol{\xi}_i^T = 0,\ i = 1,2,\mathbf{L}\ ,N \tag{6}$$

Bring the formula (4) and the formula (5) into the formula (6) to obtain:

$$\left(\frac{\mathbf{I}}{\mathbf{C}} + \mathbf{H}\mathbf{H}^T\right)\boldsymbol{\alpha} = \mathbf{T} \tag{7}$$

By the formula (4) and the formula (7), the formula (8) can get:

$$\boldsymbol{\beta} = \mathbf{H}^T\left(\frac{\mathbf{I}}{\mathbf{C}} + \mathbf{H}\mathbf{H}^T\right)^{-1}\mathbf{T} \tag{8}$$

The output function for the ELM classifier can be expressed as:

$$\mathbf{f}(\mathbf{x}) = \mathbf{h}(\mathbf{x})\boldsymbol{\beta} = \mathbf{h}(\mathbf{x})\mathbf{H}^T\left(\frac{\mathbf{I}}{\mathbf{C}} + \mathbf{H}\mathbf{H}^T\right)^{-1}\mathbf{T} \tag{9}$$

The definition of the kernel matrix of the ELM is shown as follows:

$$\boldsymbol{\Omega}_{ELM} = \mathbf{H}\mathbf{H}^T : \boldsymbol{\Omega}_{ELM_{ij}} = h(\mathbf{x}_i)h(\mathbf{x}_j) = K(\mathbf{x}_i, \mathbf{x}_j) \tag{10}$$

The output function of the ELM can be expressed as the kernel form:

$$\mathbf{f}(\mathbf{x}) = \mathbf{h}(\mathbf{x})\mathbf{H}^T\left(\frac{\mathbf{I}}{C} + \mathbf{H}\mathbf{H}^T\right)\mathbf{T} = \begin{bmatrix} K(\mathbf{x},\mathbf{x}_1) \\ K(\mathbf{x},\mathbf{x}_2) \\ \mathbf{M} \\ K(\mathbf{x},\mathbf{x}_N) \end{bmatrix}\left(\frac{\mathbf{I}}{C} + \boldsymbol{\Omega}_{ELM}\right)^{-1}\mathbf{T} \tag{11}$$

The K-ELM does not need to give the activation function $h(\mathbf{x})$ and the number L of hidden layer nodes. It only needs to give the corresponding kernel function $K(\mathbf{x}_i, \mathbf{x}_j)$ to learn.

After the K-ELM completes the training, the given test sample $\mathbf{x}$ is used as the input of the classifier. The output node sequence number corresponding to the highest output value can be used to forecast class labels for the given test sample. The output function for the $i\,th$ output node is represented by $f_i(\mathbf{x})$. The prediction category label of the data $\mathbf{x}$ is:

$$label(\mathbf{x}) = \arg\max_{i\in\{1,2,\mathbf{L}\ ,m\}} f_i(\mathbf{x}) \tag{12}$$

B. Online Sequential Extreme Learning Machine

To apply to online sequence data, Nan-Ying Liang et al. [37] proposed OS-ELM and realized online learning of ELM based-on the recursive least square (RLS) method.

The OS-ELM learning process includes two learning stages: the initialization stage and the online learning stage. In the initialization stage, the quantity of dataset is selected to be

higher than the quantity of the hidden layer nodes ($N_0 \geq \tilde{N}$), and the initial reference value is obtained by training. After initialization, the data is entered one by one, and OS-ELM enters the online learning phase. In the online learning phase, only the current incoming data is used to update the output weight. After the data is used, it will be discarded and no more used. The training time is shortened without repeated use.

The learning procedure of OS-ELM is as follows:

First, the type of the hidden layer node and the activation function $g(x)$ are selected. The number $\tilde{N}$ of hidden layer nodes and the data set $N=\left\{\left(\mathbf{x}_i,\mathbf{t}_i\right)\mid \mathbf{x}_i\in\mathbf{R}^n,\mathbf{t}_i\in\mathbf{R}^m,i=1,2,\mathbf{L}\ ,N\right\}$ are set.

The first stage: initialization of learning.

A small piece of training data $C_0=\left\{\left(\mathbf{x}_i,\mathbf{t}_i\right)\right\}_{i=1}^{N_0}$ is selected to enter the OS-ELM. Where, $N_0\geq\tilde{N}$.

(1) Randomly generate initial parameters $\mathbf{w}_i$ and b_i . Where, $i=1,2,\cdots,\tilde{N}$. When nodes are added, $\mathbf{w}_i$ and b_i are input weights and thresholds respectively. In the case of radial basis function (RBF) nodes, $\mathbf{w}_i$ and b_i are center and width respectively.

(2) The output matrix of the initial hidden layer is calculated as the formula (13):

$$\mathbf{H}_0=\begin{pmatrix} g\left(\mathbf{w}_1\mathbf{x}_1+b_1\right) & g\left(\mathbf{w}_2\mathbf{x}_1+b_2\right) & \cdots & g\left(\mathbf{w}_{\tilde{N}}\mathbf{x}_1+b_{\tilde{N}}\right)\\ g\left(\mathbf{w}_1\mathbf{x}_2+b_1\right) & g\left(\mathbf{w}_2\mathbf{x}_2+b_2\right) & \cdots & g\left(\mathbf{w}_{\tilde{N}}\mathbf{x}_2+b_{\tilde{N}}\right)\\ \vdots & \vdots & \ddots & \vdots\\ g\left(\mathbf{w}_1\mathbf{x}_{N_0}+b_1\right) & g\left(\mathbf{w}_2\mathbf{x}_{N_0}+b_2\right) & \cdots & g\left(\mathbf{w}_{\tilde{N}}\mathbf{x}_{N_0}+b_{\tilde{N}}\right)\end{pmatrix}_{N_0\times\tilde{N}} \tag{13}$$

(3) The premier output weight $\boldsymbol{\beta}_0$ is calculated, as shown in the formula (14):

$$\boldsymbol{\beta}_0=\mathbf{M}_0\mathbf{H}_0^T\mathbf{T}_0 \tag{14}$$

Where:

$$\mathbf{M}_0=\left(\mathbf{H}_0^T\mathbf{H}_0\right)^{-1} \tag{15}$$

$$\mathbf{T}_0=\left[\mathbf{t}_1,\mathbf{t}_2,\mathbf{L}\ ,\mathbf{t}_{N_0}\right]^T \tag{16}$$

(4) $k=0$. Where k are the quantities of blocks.

The second stage: online learning.

When the $k+1th$ sample set C_{k+1} arrives, N_{k+1} represents the sample size of the $k+1th$ block and $C_{k+1}=\left\{\left(\mathbf{x}_i,\mathbf{t}_i\right)\right\}_{i=(\sum_{j=0}^{k}N_j)+1}^{\sum_{j=0}^{k+1}N_j}$.

(1) For the N_{k+1} data in the $k+1th$ block, the output matrix $\mathbf{H}_{k+1}$ of the partially hidden layer is calculated, as shown in the formula (17):

$$\mathbf{H}_{k+1}=\begin{pmatrix} g\left(\mathbf{w}_1\mathbf{x}_{\left(\sum_{i=0}^{k}N_j+1\right)}+b_1\right) & g\left(\mathbf{w}_2\mathbf{x}_{\left(\sum_{i=0}^{k}N_j+1\right)}+b_2\right) & \cdots & g\left(\mathbf{w}_{\tilde{N}}\mathbf{x}_{\left(\sum_{i=0}^{k}N_j+1\right)}+b_{\tilde{N}}\right)\\ g\left(\mathbf{w}_1\mathbf{x}_{\left(\sum_{i=0}^{k}N_j+2\right)}+b_1\right) & g\left(\mathbf{w}_2\mathbf{x}_{\left(\sum_{i=0}^{k}N_j+2\right)}+b_2\right) & \cdots & g\left(\mathbf{w}_{\tilde{N}}\mathbf{x}_{\left(\sum_{i=0}^{k}N_j+2\right)}+b_{\tilde{N}}\right)\\ \vdots & \vdots & \ddots & \vdots\\ g\left(\mathbf{w}_1\mathbf{x}_{\left(\sum_{i=0}^{k+1}N_j\right)}+b_1\right) & g\left(\mathbf{w}_2\mathbf{x}_{\left(\sum_{i=0}^{k+1}N_j\right)}+b_2\right) & \cdots & g\left(\mathbf{w}_{\tilde{N}}\mathbf{x}_{\left(\sum_{i=0}^{k+1}N_j\right)}+b_{\tilde{N}}\right)\end{pmatrix}_{N_{k+1}\times\tilde{N}} \tag{17}$$

(2) The output weight $\boldsymbol{\beta}_{k+1}$ of the training sample of the $k+1$ *th* block is calculated, as shown in the formula (18):

$$\boldsymbol{\beta}_{k+1}=\boldsymbol{\beta}_k+\mathbf{M}_{k+1}\mathbf{H}_{k+1}^T\left(\mathbf{T}_{k+1}-\mathbf{H}_{k+1}\boldsymbol{\beta}_k\right) \tag{18}$$

Where:

$$\mathbf{M}_{k+1}=\mathbf{M}_k-\mathbf{M}_k\mathbf{H}_{k+1}^T\left(\mathbf{I}+\mathbf{H}_{k+1}\mathbf{M}_k\mathbf{H}_{k+1}^T\right)^{-1}\mathbf{H}_{k+1}\mathbf{M}_k \tag{19}$$

(3) $k=k+1$.

After online learning, the output weight is $\boldsymbol{\beta}_{k+1}$.

IV. Fusion Model for Failure Diagnosis of the PEMFC System Based on Data Fusion

The fault diagnosis of the PEMFC system is prone to be misdiagnosed by a single method. Therefore, it is necessary to associate the consequences of other fault diagnosis approaches to improve the accuracy of fault diagnosis.

A. Dempster-Shafer Evidence Theory

The D-S evidence theory uses the mathematical derivation method to perform the fusion calculation of inaccurate and incomplete information. In the fusion algorithm of Dempster-Shafer evidence theory, the recognition framework is the framework of the whole judgment, and the underlying probability distribution is the basis of fusion. The synthesis rule is the fusion process. The likelihood function and trust function are adapted to express the lower and upper bounds of the support strength of the fusion conclusion on the assumption.

Θ is a mutually exclusive and non-empty finite set, which is called the recognition framework. Under this framework, all possible hypotheses for a particular time are included. For example, there is a recognition framework that can be expressed as: $\Theta=\left\{F_1,F_2,\cdots,F_n\right\}$. There are n possible hypotheses in the identification framework. F_1 means "Suppose F_1 appears". The task of the fusion algorithm of Dempster-Shafer evidence theory is to estimate the trusted strength of each possible tentative.

The BPA is a function, which is called the m function:

$$m:2^{\Theta}\rightarrow[0,1] \tag{20}$$

Moreover, satisfy:

$$m(\phi)=0\ \sum_{X\subseteq\Theta}m(X)=1 \tag{21}$$

When evidence is constituted, every possible assumption or combination of assumptions within the framework should be assigned a level of trust between [0, 1]. The sum of the trust level of the hypothetical or hypothetical combination should be equal to 1. The fusion conclusion of Dempster-Shafer evidence theory expresses the support strength to any hypothesis through an interval. The lower bound of this interval is called the trust function. The trust function is also named the Belief function (Bel). The trust function on the recognition framework Θ is defined as:

$$Bel(A)=\sum_{B\subseteq A}m(B) \tag{22}$$

The trust function of one hypothesis in the fusion conclusion only calculates the support strength of the hypothesis directly in

the integration calculation and doesn't calculate the support strength in combination with the hypothesis. If a part of the support strength in the underlying probability distribution is assigned to an unknown domain, then the support strength of this part cannot be calculated in the trust function.

The upper bound of the fusion conclusion interval of Dempster-Shafer evidence theory is called the plausibility function (PI). The PI on the recognition framework Θ is shown as:

$$Pl(A) = \sum_{B \mathbf{I}\, A \neq \varnothing} m(B) \tag{23}$$

The likelihood function of a hypothesis in the fusion conclusion not only calculates the support strength for the hypothesis directly in the fusion calculation but also calculates the support strength of the combination containing the hypothesis and the support strength assigned to the unknown domain.

In D-S evidence theory, for a hypothesis A in the identification framework Θ, the likelihood function $Pl(A)$ and the trust function $Bel(A)$ by the BPAs are calculated respectively to form the trust interval $\left[Bel(A), Pl(A)\right]$. It is used to indicate the confirmation degree of a hypothesis, as shown in Fig. 4.

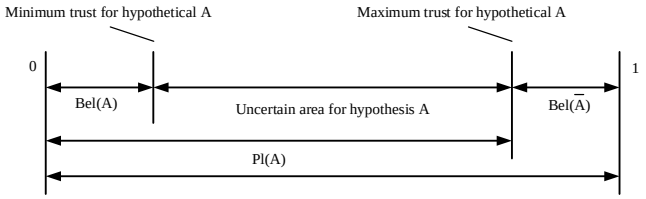

Fig. 4 The relationship between the likelihood function and the trust function

There is a relationship between the likelihood function and the trust function as follows:

$$Pl(X) \geq Bel(X) \quad Pl(X) = 1 - Bel\left(\overline{X}\right) \tag{24}$$

The fusion conclusion can be used to express the support strength for each possible hypothesis by using the trust function, likelihood function or the interval composed of trust function and likelihood function.

Dempster's combinational rule is also called evidence synthesis formulas, which can be expressed in the following expressions:

$$m(C) = m_i(X) \oplus m_j(Y) = \begin{cases} 0 & X \mathbf{I}\, Y = \varnothing \\ \dfrac{\sum_{X \mathbf{I} Y = \varnothing, \forall X, Y \subseteq \Theta} m_i(X) \times m_j(Y)}{1 - \sum_{X \mathbf{I} Y = \varnothing, \forall X, Y \subseteq \Theta} m_i(X) \times m_j(Y)} & X \mathbf{I}\, Y \neq \varnothing \end{cases} \quad i, j = 1, 2, \mathbf{L}\ , m \tag{25}$$

B. Fusion Model for Fault Diagnosis of the PEMFC System Based on Data Fusion

In practical cases, PEMFC systems are diagnosed through a single method. It is inevitable that there will be fault misjudgment. The integration results of the several diagnostic methods are taken into account to improve the classification accuracy of failure diagnosis. The numerical output of traditional ELM cannot be used as input of Dempster-Shafer evidence theory. It is necessary to transform the digital output of traditional ELM into the probabilistic output. In order to realize the decision-level fusion ELM, it is necessary to use the squashing function to convert the traditional ELM output into the probabilistic output, so that the decision results of different characteristics are unified in the fixed range.

Decision-level fusion first acquires data from each sensor and performs initial decision after extracting its features. Then, the decision results are correlated, and the fusion of local decision is completed in the fusion center. The first question that the decision-level fusion ELM needs to solve is how to unify the output range of all ELMs. In order to get the probability output, the output of the standard ELM is mapped to the posterior probability by a squeezing function:

$$P\left(\mathbf{f_i}(\mathbf{x})\right) = \frac{1}{1 + \exp\left(-\mathbf{f_i}(\mathbf{x})\right)},\ i = 1, 2, \mathbf{L}\ , m \tag{26}$$

Furthermore, the probability of the input sample $\mathbf{x}$ in the label i is given in mathematical sense, which is recorded as $p_i(\mathbf{x})$:

$$p_i(\mathbf{x}) = \frac{P\left(\mathbf{f}_i(\mathbf{x})\right)}{\sum_{i=1}^{m} P\left(\mathbf{f_i}(\mathbf{x})\right)} \tag{27}$$

For the multi-classification problem with label m class, when the M-group classifier is used for decision fusion, the probability output matrix can be calculated:

$$\mathbf{P}(\mathbf{x}) = \begin{pmatrix} p_{11}(\mathbf{x}) & p_{12}(\mathbf{x}) & \cdots & p_{1M}(\mathbf{x}) \\ p_{21}(\mathbf{x}) & p_{22}(\mathbf{x}) & \cdots & p_{2M}(\mathbf{x}) \\ \vdots & \vdots & \ddots & \vdots \\ p_{m1}(\mathbf{x}) & p_{m1}(\mathbf{x}) & \cdots & p_{mM}(\mathbf{x}) \end{pmatrix}_{m \times M} \tag{28}$$

Each column in the matrix corresponds to the probability output of a set of classifiers. The element $p_{ik}(\mathbf{x})$ of the matrix refers to the input sample $\mathbf{x}$. The *k th* group classifier determines the probability that it belongs to a class i. After the probability output matrix is obtained, the output range of the traditional ELM is treated as normalized, and the output less than zero also has a statistical significance.

Based on the above analysis results, the fusion model for failure diagnosis of the PEMFC system based on data fusion is established as shown in Fig. 5.

This article has been accepted for publication in a future issue of this journal, but has not been fully edited. Content may change prior to final publication. Citation information: DOI 10.1109/TTE.2018.2886153, IEEE Transactions on Transportation Electrification

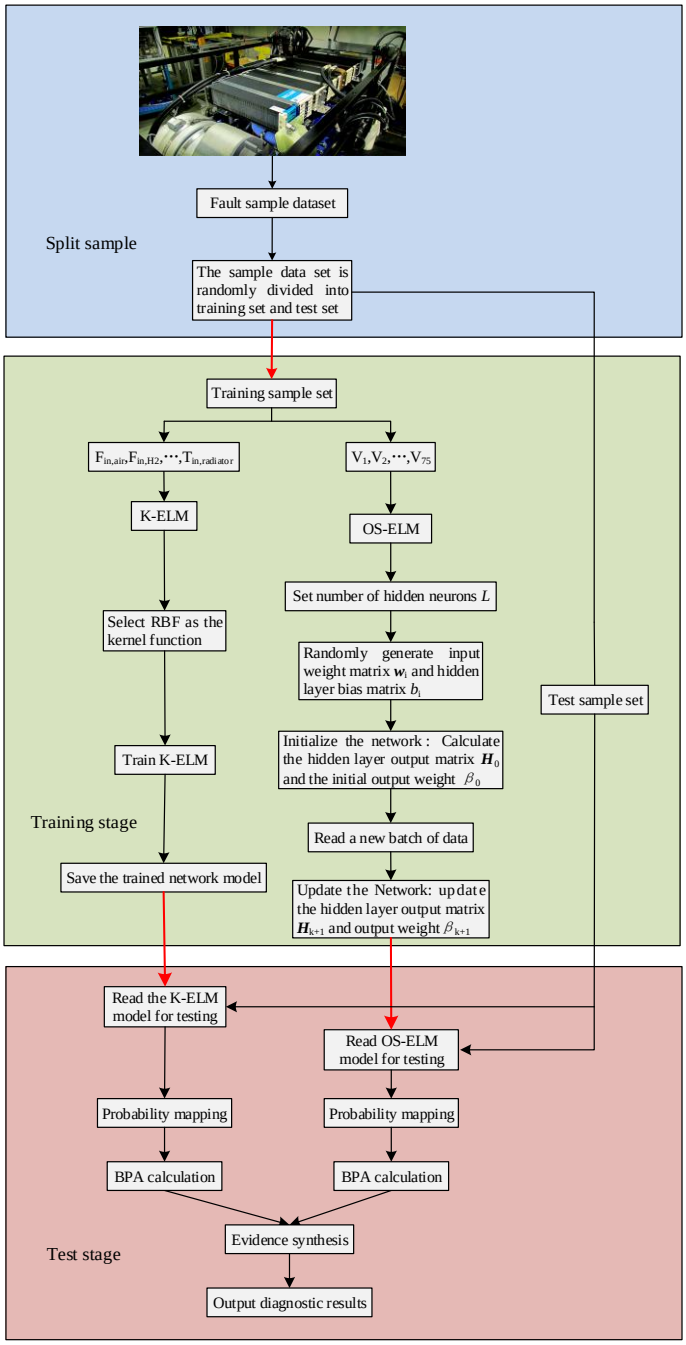

Fig. 5 Fusion model for failure diagnosis of the PEMFC system based on data fusion

V. Experimental Verification

A. Preparing Data

In order to validate the effectiveness of the proposed failure diagnosis approach, it is necessary to collect a set number of training and test datasets. The first objective of this research work is to grow a failure diagnosis model of the PEMFC system based on electrical quantities and non-electrical quantities to identify the high air stoichiometry failures. After the initial fault diagnosis, the second purpose of the work is to perform the fusion diagnostic output of the initial diagnosis result by Dempster-Shafer evidence theory. The feasibility of data fusion diagnosis method is explored.

In order to identify and validate the model, the real data is obtained from the 14.4 kW liquid-cooled fuel cell test platform built in the laboratory. The dataset contains four different degrees of high air stoichiometry failure states. The fault sample dataset is shown in Table 5.

Table 5 Fault sample dataset

Fault type	Air stoichiometry	Training set	Test set
F1	5.1	60	33
F2	4.6	25	10
F3	4.2	60	34
F4	2.1	155	77

B. Selection of the Variables for Diagnosis

Seventy-five single cell voltages are selected as the characteristic electrical quantities. The non-electrical quantities selected are shown in Table 6.

Table 6 Selected non-electrical quantities

Variable	Notation
The flow rate at the H_2 inlet	F_{in,H_2}
The pressure at the H_2 inlet	P_{in,H_2}
The temperature at the H_2 inlet	$T_{in.H_2}$
The flow rate at the air inlet	$F_{in,air}$
The pressure at the air inlet	$P_{in,air}$
The temperature at the air inlet	$T_{in,air}$
Flow rate at the coolant inlet	$F_{in,water}$
The pressure at the coolant inlet	$P_{in,water}$
The temperature at the coolant inlet	$T_{in,water}$
The temperature at the coolant outlet	$T_{out,water}$
The temperature at the radiator inlet	$T_{in,radiator}$

C. Fault Diagnosis of PEMFC System Based on Electrical Quantities and Non-electrical Quantities

1) Fault Diagnosis of PEMFC System Based on Electrical Quantities

A large number of field practice and theoretical research show that the voltage distribution of a single cell is closely related to the fault type and fault level of the fuel cell system. To some extent, the voltage distribution of a single cell can glass the running state of the PEMFC system. Seventy-five single cell voltage values are selected as the OS-ELM input.

Table 7 Parameter table of OS-ELM

Parameter	Notation	Value
The number of hidden layer neurons	L	100
The quantity of initial training data adopted at the initial phase	$N0$	280
Size of a block of data learned at each step	$Block$	20

During the implementation of the OS-ELM algorithm, some arguments need to be manually set. The algorithm stipulates that the quantity of initial training data adopted at the initial phase must not be less than the number of hidden neurons. When the numbers of initial training data adopted at the initial phase and the numbers of hidden neurons are specific, the influence of the size of the block of data learned at each step on the training accuracy can be ignored. According to the parameter characteristics of the above OS-ELM, the numbers of hidden neurons, the initial training data adopted at the initial phase and the size of the block of data learned at each step are

set respectively. The parameters of OS-ELM are shown in Table 7. The RBF is adopted as the activation function.

The fault identification results of the PEMFC training data are presented in Fig. 6(a). Here, the horizontal axis expresses the 300 training data, while the vertical axis expresses the four fault type of the PEMFC. The classification accuracy rate is defined as the rate between the quantity of the right diagnosed data and the total quantity of the data. It serves to show the diagnosis rate is 100% for the PEMFC training dataset by the OS-ELM model.

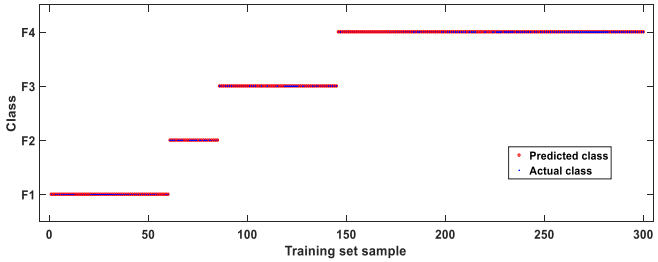

(a) Diagnosis results of the training sample

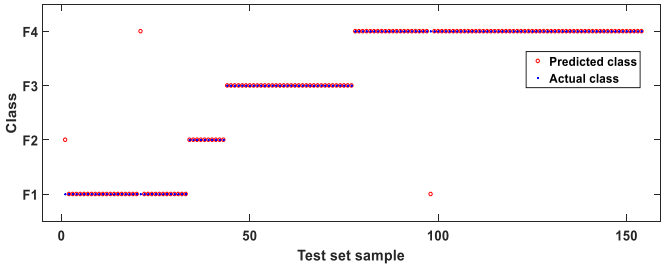

(b) Diagnosis results of the test sample

Fig. 6 Failure diagnosis of PEMFC system based on the OS-ELM

Diagnosis results of the PEMFC system datasets are shown in Fig. 6(b) and Table 8. In Fig. 6(b), the horizontal axis expresses the 154 test samples, and the significance of the vertical axis is equally as the y-axis of Fig. 6(a). Only 3 of the 154 test dataset is error diagnostics, and the diagnostic accuracy is at most 98.05%. The classification accuracies corresponding to the F1 state, the F2 state, the F3 state, and the F4 state are 93.94%, 100%, 100%, and 98.70% respectively. At list in Table 8, the summation of the test time and the training time is 0.0731 s. The experimental results clarify that the OS-ELM model is a practical approach to diagnose PEMFC faults.

Table 8 Diagnostic results based on the OS-ELM

Training time	Test time	Classification accuracy of the training set	Classification accuracy of the test set
0.0625 s	0.0106 s	100%	98.05%

2) Fault Diagnosis of PEMFC System Based on Non-electrical Quantities

The operation parameters of the PEMFC system contain an abundant message about the states of the PEMFC system. The values of 11 kinds of non-electrical quantities in Table 6 are selected as the fault parameters of the K-ELM.

The input feature vector x of the K-ELM selected in this paper can be expressed as:

$$x=\left(x_1,x_2,\cdots,x_{11}\right) \tag{29}$$

Where, $x_i\in[0,1]$, $i=1,2,\cdots,11$. x corresponds to the 11 attributes of the input variables. Thus, the number of K-ELM input neurons is 11.

The fault states of four different degrees of high air stoichiometries are represented by $t_1\sim t_4$ respectively. Then the theoretical output vector t_p of K-ELM is $[t_1,t_2,t_3,t_4]$. Because the RBF kernel function is simple and has few parameters, it is usually selected as a kernel function by K-ELM. Different kernel functions are applied to different problems. However, there are no uniform standards for the choice of the kernel function. In the general multi-classification problem, since the RBF kernel function has only one kernel parameter and it can be applied to arbitrarily distributed samples with universal applicability, so the RBF kernel function is chosen in this paper. The kernel function of K-ELM is set as the RBF kernel function.

The fault identification results of the PEMFC training dataset are presented in Fig. 7(a). It serves to show the diagnostic accuracy is 100% for the PEMFC training dataset by the K-ELM model.

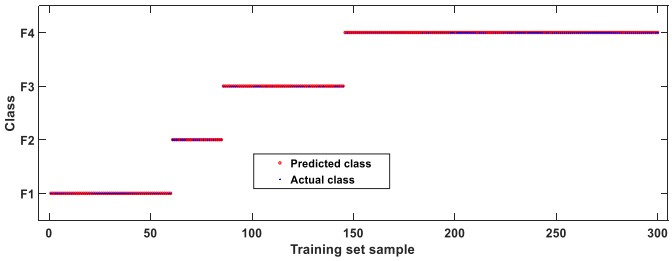

(a) Diagnosis results of the training sample

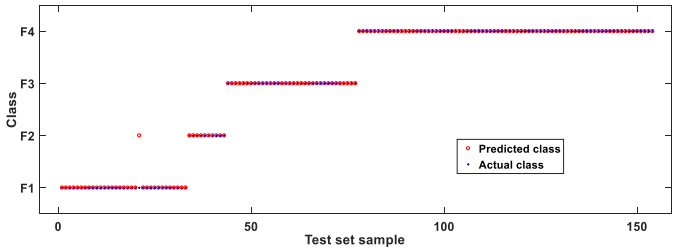

(b) Diagnosis results of the test sample

Fig. 7 Failure diagnosis of PEMFC system based on the K-ELM

The diagnosis results of the PEMFC system are shown in Fig. 7(b) and Table 9. Only 1 of the 154 test set is error diagnostics, and the diagnostic accuracy is at most 99.35%. The classification accuracies corresponding to the F1 state, the F2 state, the F3 state, and the F4 state are 96.97%, 100%, 100%, and 100% respectively. At list in Table 9, the sum of the training time and the test time is 0.0505 s. The experimental consequences clarify that the K-ELM model is also an available method to detect the PEMFC failures.

Table 9 Diagnostic results based on the K-KLM

Training time	Test time	Classification accuracy of the training set	Classification accuracy of the test set
0.0459 s	0.0046 s	100%	99.35%

D. Fault Diagnosis of PEMFC System Based on D-S Evidence Theory

After the fault diagnosis model of PEMFC system based on the electrical quantities and the non-electrical quantities is established, the diagnostic results of the above two strategies are converted to the BPA function by the formula (26) ~

This article has been accepted for publication in a future issue of this journal, but has not been fully edited. Content may change prior to final publication. Citation information: DOI 10.1109/TTE.2018.2886153, IEEE Transactions on Transportation Electrification

formula (27). Dempster-Shafer evidence theory algorithm is used to make fusion diagnosis output at the decision layer.

The diagnostic results of the PEMFC system datasets are described in Fig. 8(b) and Table 10. Only 2 of the 154 test sets is error diagnostics, and the diagnostic accuracy is at the outside 98.70%. The classification accuracies corresponding to the F1 state, the F2 state, the F3 state, and the F4 state are 93.94%, 100%, 100%, and 100% respectively. At list in Table 10, the test time is 0.0781 s. The experimental results illustrate that the Dempster-Shafer evidence theory is a valid approach to diagnose the PEMFC failures, too.

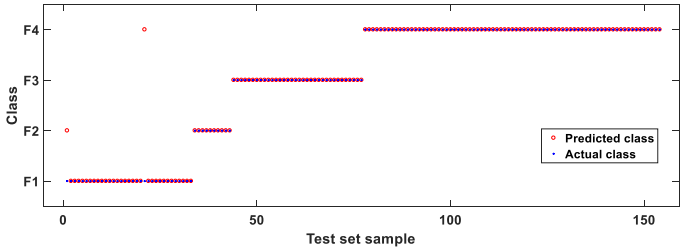

Fig. 8 Fault diagnosis of PEMFC system based on the D-S evidence theory

Table 10 Diagnostic results based on the D-S evidence theory

Test time	Classification accuracy of the test set
0.0781 s	98.70%

In summary, the fast fault diagnosis method of the PEMFC system based on data fusion proposed in this paper has the characteristics of short running time and high classification accuracy. The total running time of the entire program is 0.2011 s, and the diagnostic accuracy of the test set is 98.70%. Two data of the F1 state are error diagnostics. One data of the F1 state is wrongly diagnosed as an F2 state, one group of the F1 state is wrongly diagnosed as an F4 state.

E. Comparison with the Available Approaches

For further proving the reliability of the novel method, it is necessary to compare the novel approach with the algorithms of the existing papers. In this paper, one-against-one SVM [13] and BPNN [16] are respectively chosen as the control group. In order to ensure the fairness of the algorithm contrast, the same data set of fault diagnosis and the same computer (CPU@2.8GHz，RAM@8GB，MATLAB 2016b 64-bit environment) are adopted by the novel method and the control group.

1) Fault Diagnosis of PEMFC System Based on the One-against-one SVM

In order to accelerate the convergence speed of the program and ensure the comparability between the variables, the selected fault feature vectors need to be normalized:

$$y_i = \frac{x_i - x_{\min}}{x_{\max} - x_{\min}},\ i = 1, 2, \mathbf{L}\ , N \tag{30}$$

Where x_i is the diagnostic variable before conversion; y_i is the diagnostic variable after normalization; $x_{\min}$ is the minimal value of the dataset; $x_{\max}$ is the highest value of the dataset; N is the length of the data.

A total of eighty-six property values of electrical quantities and non-electrical quantities are normalized. The RBF is adopted as the kernel function. The cross-validation (CV) approach is adopted to search for the best kernel function parameter g and the best penalty parameter c. When the performance of the model is the same, to reduce the calculation time, the combination of the parameters with a smaller penalty factor c is preferred. Because the penalty factor c is larger, the quantity of support vectors is even more, and the calculation amount is more considerable.

The fault identification results of the PEMFC training dataset are described in Fig. 9(a). It serves to show the prediction accuracy is 99.67% for the PEMFC training dataset by the one-against-one SVM.

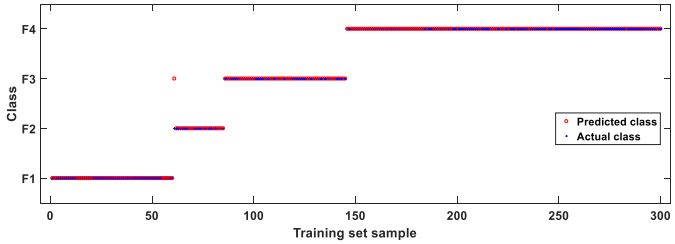

(a) Diagnostic results of the training sample

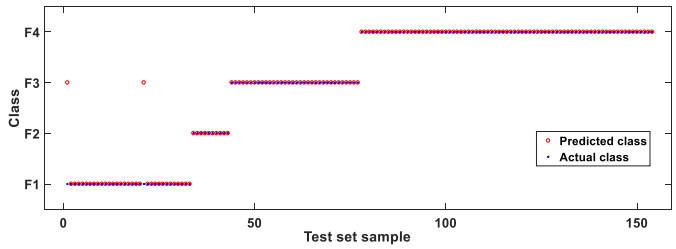

(b) Diagnostic results of the test sample

Fig. 9 Failure diagnosis of PEMFC system ground on the one-against-one SVM

The diagnostic results of the PEMFC system are described in Fig. 9(b) and Table 11. Only 2 of the 154 test samples is error detection, and the correct detection rate is at the most 98.70%. The classification accuracies corresponding to the F1 state, the F2 state, the F3 state, and the F4 state are 93.94%, 100%, 100%, and 100% respectively. At list in Table 11, the running time is 484.97 s.

Table 11 Diagnostic results based on the one-against-one SVM

Running time	Penalty parameter c	Kernel function parameter g	Classification accuracy of the training set	Classification accuracy of the test set
484.97 s	2	0.082	99.67%	98.70%

2) Fault Diagnosis of PEMFC System Based on BPNN

In the three-layer network, there is a close connection between the number n_1 of input layer neurons and the number n_2 of hidden layer neurons:

$$n_2 = 2 \times n_1 + 1 \tag{31}$$

There are eight-six input parameters and four output parameters for the samples of the electrical quantities and non-electrical quantities. The n_2 value is 173. The neural network structure is 86-173-4, that is, there are 86 nodes at the input layer, 173 nodes at the hidden layer and four nodes at the output layer. The structure of BPNN is shown in Fig. 10. Mean square error (MSE) is used as the network performance function of BPNN. The process of network learning is to make the error reach the design goal. The learning algorithm based on Levenberg-Marquardt is adopted, and the error target of

This article has been accepted for publication in a future issue of this journal, but has not been fully edited. Content may change prior to final publication. Citation information: DOI 10.1109/TTE.2018.2886153, IEEE Transactions on Transportation Electrification

training is 0.001. The hyperbolic tangent S type transfer function (tansig) is adopted as the transport function of the hidden layer. The linear transfer function (purelin) is selected as the transfer function of the output layer. All data samples need to be normalized before the network is trained. It is avoided that the error of fault diagnosis structure is magnified due to the magnitude of differences between different kinds of data sets.

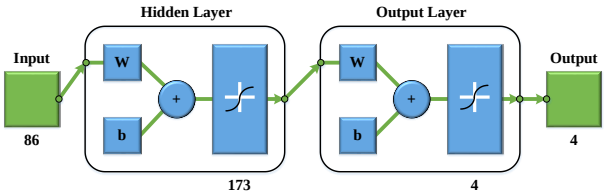

Fig. 10 The structure of BPNN

The Fault identification results of the PEMFC training dataset are as shown in Fig. 11(a). It serves to show the correct detection rate is 99.67% for the PEMFC training dataset by the BPNN model.

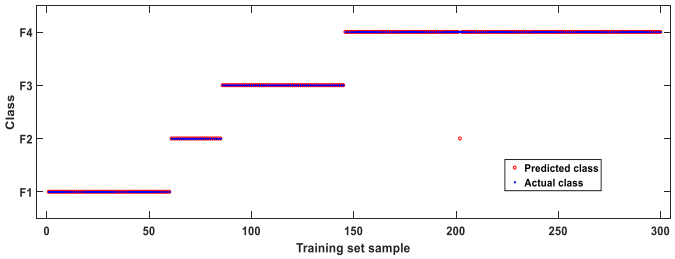

(a) Classification results of the training sample

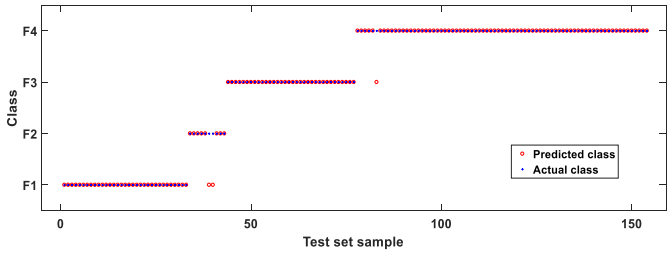

(b) Diagnostic results of the test sample

Fig. 11 Fault diagnosis of PEMFC system based on the BPNN

The results of classification for the PEMFC system are shown in Fig. 11(b) and Table 12. Only 3 of 154 test data is error diagnostics, and the correct detection rate is at best 98.05%. The first column represents the running time of the fault diagnostic datasets. The classification accuracies of the F1 state, the F2 state, the F3 state, and the F4 state are 100%, 80%, 100%, and 98.70% respectively. At list in Table Table 12, the running time is 3128.5 s.

Table 12 Diagnostic results based on the BPNN

Running time	Classification accuracy of the training set	Classification accuracy of the test set
3128.5 s	99.67%	98.05%

3) Comparative Analysis

Table 13 Comparison of the results of three kinds of diagnostic methods

Diagnostic method	Parameter	Value	Running time	Classification accuracy of the training set	Classification accuracy of the test set
Data fusion method	(N0, L, Block)	(280, 100, 20)	0.2011 s	100%	98.70%
One-against-one SVM	(c, g)	(2, 0.082)	484.79 s	99.67%	98.70%
BPNN	N	86	3128.5 s	99.67%	98.05%

The comparison of the results of three kinds of diagnostic methods is shown in Table 13.

a) Comparison of Recognition Accuracy

In 454 groups of fault diagnosis samples with different degrees of high air stoichiometries, 300 groups of data are respectively selected as training samples to train the data fusion model, one-against-one SVM and BPNN. The remaining 154 sets of data are adopted as a pattern recognition test set to test the recognition results of the above algorithms separately. From Table 13, the diagnostic accuracy of the test samples and the classification accuracy of the training samples of the data fusion method are both the highest. Although the recognition rate of the test set of the one-against-one SVM is very high, there is a case of misdiagnosis of the training set. Also, the diagnostic accuracies of the test set and a training set of BPNN are both lower than that of data fusion model. The comparison shows that the data fusion method is beneficial for the pattern recognition of the PEMFC system.

b) Comparison of Running Time Performance

Because the hidden layer bias matrix and the input weight matrix of the ELM algorithm are casually created, the problems of repeatedly training and modifying connection weights and thresholds are avoided. On the other hand, the input weight matrix is necessarily an optimal solution to minimize the loss function by using the least square method, so there is no need for the iterative process. Therefore, the ELM algorithm can significantly reduce the adjustment time of network training and has a breakneck training speed.

For the K-ELM algorithm, the selected kernel function is the RBF kernel function. For the OS-ELM algorithm, the number *N0* of the initial training data adopted in the initial phase is 280, the number *L* of hidden neurons is 100, the size *Block* of a block of the data learned at each step is 173.

From Table 13, it can be seen that the data fusion model has a more significant advantage than the one-against-one SVM and BPNN. In the case of the same training sample, the running time of SVM is 2410 times of the data fusion algorithm. The operation time of BPNN is 15557 times of the data fusion arithmetic. The experimental consequences show that the data fusion arithmetic devised in this paper can improve the operation speed significantly while ensuring the accuracy of recognition.

VI. CONCLUSION

To realize the fast failure diagnosis of a PEMFC system, a novel failure diagnosis method of PEMFC systems based on data fusion is proposed, which combines ELM and Dempster-Shafer evidence theory. The characteristic vector extraction is carried out on the electrical quantities and the non-electrical quantities of the PEMFC system under four different faults. The K-ELM algorithm and OS-ELM algorithm are respectively used to establish the fault diagnosis model of PEMFC system based on electrical quantities and non-electrical quantities. It is used for preliminary failure

diagnosis of the PEMFC system. The diagnosis results of the above two strategies are converted into the function values of the basic probability assignment by the squeeze function. The D-S evidence theory algorithm is used to fuse the diagnostic output at the decision level.

The classification results of 154 samples of PEMFC system show that the novel method can diagnose four different degrees of high air stoichiometry failures. The average recognition rate is 98.70% and the operation time is only 0.2011 s. At the same time, the comparison with the one-against-one SVM and BPNN shows that the data fusion algorithm can significantly improve the running speed while ensuring the correct recognition rate. The novel method has the advantages of high diagnostic accuracy and fast operation speed without the data preprocessing. It can be used for online failure diagnosis of the PEMFC system.

REFERENCES

[1] D. Zhou, F. Gao, E. Breaz, A. Ravey, A. Miraoui, and K. Zhang, "Dynamic Phenomena Coupling Analysis and Modeling of Proton Exchange Membrane Fuel Cells," IEEE T. Energy Conver., 31, pp. 1399-1412, (2016).

[2] Changjun Xie, Xinyi Xu, Piotr Bujlo, Di Shen, Hengbing Zhao, and Shuhai Quan, "Fuel cell and lithium iron phosphate battery hybrid powertrain with an ultracapacitor bank using direct parallel structure," J. Power Sources, 279, pp. 487-494, (2015).

[3] Junbo Jia, Gucheng Wang, Yew Thean Cham, Youyi Wang, and Ming Han, "Electrical characteristic study of a hybrid PEMFC and ultracapacitor system," IEEE T. Ind. Electron., 57, pp. 1945-1953, (2010).

[4] Jianxing Liu, Salah Laghrouche, Fayez-Shakil Ahmed, and Maxime Wack, "PEM fuel cell air-feed system observer design for automotive applications: An adaptive numerical differentiation approach," Int. J. Hydrogen Energ., 39, pp. 17210-17221, (2014).

[5] X. Wu and D. Gao, "Fault tolerance control of SOFC systems based on nonlinear model predictive control," Int. J. Hydrogen Energ., 42, pp. 2288-2308, (2017).

[6] Y. Han, Q. Li, T. Wang, W. Chen, and L. Ma, "Multisource Coordination Energy Management Strategy Based on SOC Consensus for a PEMFC – Battery – Supercapacitor Hybrid Tramway," IEEE T. Veh. Technol., 67, pp. 296-305, (2018).

[7] J. Liu, Y. Gao, X. Su, M. Wack, and L. Wu, "Disturbance-Observer-Based Control for Air Management of PEM Fuel Cell Systems via Sliding Mode Technique," IEEE T. Contr. Syst. T., PP, pp. 1-10, (2018).

[8] X. Li, G. Cao and X. Zhu, "Modeling and control of PEMFC based on least squares support vector machines," Energ. Convers. Manage., 47, pp. 1032-1050, (2006).

[9] T. Wang, L. Qi, Y. Qiu, L. Yin, L. Liu, and W. Chen, "Efficiency Extreme Point Tracking Strategy Based on FFRLS Online Identification for PEMFC System," IEEE T. Energy Conver., p. 1-1, (2018).

[10] Ling Hong, Jian Chen, Zhiyang Liu, Lianghui Huang, and Zhongle Wu, "A nonlinear control strategy for fuel delivery in PEM fuel cells considering nitrogen permeation," Int. J. Hydrogen Energ., 42, pp. 1565-1576, (2017).

[11] J. Chen, Z. Liu, F. Wang, Q. Ouyang, and H. Su, "Optimal Oxygen Excess Ratio Control for PEM Fuel Cells," IEEE T. Contr. Syst. T., 26, pp. 1711-1721, (2018).

[12] J. Liu, Q. Li, W. Chen, Y. Yan, Y. Qiu, and T. Cao, "Remaining useful life prediction of PEMFC based on long short-term memory recurrent neural networks," Int. J. Hydrogen Energ., (2018).

[13] Z. Zhang, S. Li, Y. Xiao, and Y. Yang, "Intelligent simultaneous fault diagnosis for solid oxide fuel cell system based on deep learning," Appl. Energ., 233-234, pp. 930-942, (2019).

[14] L. Xu, U. Reimer, J. Li, H. Huang, Z. Hu, H. Jiang, H. Janßen, M. Ouyang, and W. Lehnert, "Design of durability test protocol for vehicular fuel cell systems operated in power-follow mode based on statistical results of on-road data," J. Power Sources, 377, pp. 59-69, (2018).

[15] Jianxing Liu, Wensheng Luo, Xiaozhan Yang, and Ligang Wu, "Robust model-based fault diagnosis for PEM fuel cell air-feed system," IEEE T. Ind. Electron., 65, pp. 3261-3269, (2016).

[16] D. Ritzberger and S. Jakubek, "Nonlinear data-driven identification of polymer electrolyte membrane fuel cells for diagnostic purposes: A Volterra series approach," J. Power Sources, 361, pp. 144-152, (2017).

[17] Z. Li, R. Outbib, S. Giurgea, D. Hissel, S. Jemei, A. Giraud, and S. Rosini, "Online implementation of SVM based fault diagnosis strategy for PEMFC systems," Appl. Energ., 164, pp. 284-293, (2016).

[18] X. Zhao, L. Xu, J. Li, C. Fang, and M. Ouyang, "Faults diagnosis for PEM fuel cell system based on multi-sensor signals and principle component analysis method," Int. J. Hydrogen Energ., 42, pp. 18524-18531, (2017).

[19] Z. Zheng, S. Morando, M. Pera, D. Hissel, L. Larger, R. Martinenghi, and A. Baylon Fuentes, "Brain-inspired computational paradigm dedicated to fault diagnosis of PEM fuel cell stack," Int. J. Hydrogen Energ., 42, pp. 5410-5425, (2017).

[20] M. Shao, X. Zhu, H. Cao, and H. Shen, "An artificial neural network ensemble method for fault diagnosis of proton exchange membrane fuel cell system," Energy, 67, pp. 268-275, (2014).

[21] J. Liu, Q. Li, W. Chen, and T. Cao, "A discrete hidden Markov model fault diagnosis strategy based on K-means clustering dedicated to PEM fuel cell systems of tramways," Int. J. Hydrogen Energ., 43, pp. 12428-12441, (2018).

[22] Z. Li, R. Outbib, S. Giurgea, and D. Hissel, "Fault diagnosis for PEMFC systems in consideration of dynamic behaviors and spatial inhomogeneity," IEEE T. Energy Conver., p. 1-1, (2018).

[23] Z. Li, C. Cadet and R. Outbib, "Diagnosis for PEMFC based on magnetic measurements and data-driven approach," IEEE T. Energy Conver., p. 1-1, (2018).

[24] L. Mao and L. Jackson, "Effect of Sensor Set Size on Polymer Electrolyte Membrane Fuel Cell Fault Diagnosis," Sensors-Basel, 18, p. 2777, (2018).

[25] L. Mao, L. Jackson and B. Davies, "Effectiveness of a Novel Sensor Selection Algorithm in PEM Fuel Cell On-Line Diagnosis," IEEE T. Ind. Electron., 65, pp. 7301-7310, (2018).

[26] L. Mao, L. Jackson and B. Davies, "Investigation of PEMFC fault diagnosis with consideration of sensor reliability," Int. J. Hydrogen Energ., 43, pp. 16941-16948, (2018).

[27] L. Mao, L. Jackson and S. Dunnett, "Fault Diagnosis of Practical Polymer Electrolyte Membrane (PEM) Fuel Cell System with Data-driven Approaches," Fuel Cells, 17, pp. 247-258, (2017).

[28] A. H. Detti, S. M. S. Jemei and N. Y. Steiner, "Classification based method using Fast Fourier Transform (FFT) and Total Harmonic Distorsion (THD) dedicated to Proton Exchange Membrane Fuel Cell (PEMFC) diagnosis," in *2017 IEEE Vehicle Power and Propulsion Conference (VPPC)*: IEEE, 2017, pp. 1-6.

[29] R. Petrone, E. Pahon, F. Harel, S. Jemei, D. Chamagne, D. Hissel, and M. C. Pera, "Data-Driven Multi-Fault Approach for H2/O2 PEM Fuel Cell Diagnosis," in *2017 IEEE Vehicle Power and Propulsion Conference (VPPC)*: IEEE, 2017, pp. 1-5.

[30] G. Buonocunto, G. Spagnuolo and W. Zamboni, "A Kalman filter based approach to PEM fuel cell fault detection," in *2017 IEEE 26th International Symposium on Industrial Electronics (ISIE)*: IEEE, 2017, pp. 934-939.

[31] E. Pahon, D. Hissel, S. Jemei, and N. Yousfi-Steiner, "Relative Wavelet Energy as a Diagnosis Tool for PEM Fuel Cells," in *2016 IEEE Vehicle Power and Propulsion Conference*: IEEE, 2016, pp. 1-6.

[32] E. Pahon, N. Yousfi Steiner, S. Jemei, D. Hissel, and P. Moçoteguy, "A signal-based method for fast PEMFC diagnosis," Appl. Energ., 165, pp. 748-758, (2016).

[33] Q. Li, T. Wang, C. Dai, W. Chen, and L. Ma, "Power Management Strategy Based on Adaptive Droop Control for a Fuel Cell-Battery-Supercapacitor Hybrid Tramway," IEEE T. Veh. Technol., 67, pp. 5658-5670, (2018).

[34] Z. Huang, Y. Yu, J. Gu, and H. Liu, "An Efficient Method for Traffic Sign Recognition Based on Extreme Learning Machine.," IEEE Transactions on Cybernetics, 47, pp. 920-933, (2017).

[35] Y. Li, X. Zhao, Z. Liu, Y. Li, W. Chen, and Q. Li, "Experimental study on the voltage uniformity for dynamic loading of a PEM fuel cell stack," Int. J. Hydrogen Energ., 40, pp. 7361-7369, (2015).

[36] B. P. S. Inc., "FCvelocity®-9SSL V4 Product Manual and Integration Guide,": Ballard Power Systems Inc., 2011, pp. 1-66.

[37] N. Y. Liang, G. B. Huang, P. Saratchandran, and N. Sundararajan, "A fast and accurate online sequential learning algorithm for feedforward networks," IEEE Trans Neural Netw, 17, pp. 1411-1423, (2006).

Jiawei Liu received his B.S. degree in electrical and information engineering from the University of Electronic Science and Technology of China, Chengdu, China, in 2015. He is now working toward the Ph.D. degree in the School of Electrical Engineering, Southwest Jiaotong University. His research interests include fuel cell fault diagnosis and remaining useful life prediction.

Qi Li (M'12–SM'15) received his B.S. degree and Ph.D. degree in Electrical Engineering School from Southwest Jiaotong University, Chengdu, China, in 2006 and 2011. He did research as visiting scholar in the School of Electrical and Electronic Engineering, Nanyang Technological University, Singapore, from 2009 and 2011. He is an IET Fellow and is a professor in the School of Electrical Engineering, Southwest Jiaotong University. His research interests include fuel cell locomotives optimal control, energy management strategy of the hybrid system, and power system stability and control.

Weirong Chen (M'99–SM'16) received his B.S degree and M.S. degree in electronic engineering from Electronic Science and Technology University, respectively in 1985 and 1988, and the Ph.D. degree in power system and its automation from Southwest Jiaotong University in 1998, Chengdu, China. He is as Senior Visiting Scholar at Brunel University in 1999, England. Currently, he is an IET Fellow and is a professor in the School of Electrical Engineering, Southwest Jiaotong University. His research interests include renewable energy and its applications, fuel cell locomotive technology, and power system control. He has published more than 120 refereed journal and conference papers, 6 books, and is the holder of more than 40 Chinese patents.

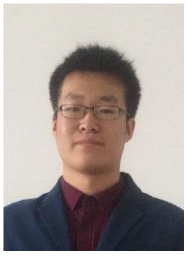

Yu Yan received his B.S. degree in Electrical Engineering School from Southwest Jiaotong University, Chengdu, China, in 2016. He is currently pursuing a doctorate in electrical engineering at Southwest Jiaotong University. His research interests include fuel cell tram optimal control, energy management strategy of the hybrid system, and multi-stack fuel cell system control.

Xiaotong Wang received her B.C. degree in the School of Electrical Engineering, Southwest Jiaotong University, Chengdu, China, in 2017. Her is currently working toward the M.S. degree in the School of Electrical Engineering, Southwest Jiaotong University, Chengdu, China. Her research interests include fault diagnosis for the fuel cell.